Complete Modeling of Nonlinear Distortion in OFDM-based Optical Wireless Communication

Dobroslav Tsonev, Sinan Sinanovic and Harald Haas

***Abstract*—This paper presents a complete analytical framework for modeling memoryless nonlinear effects in an intensity modulation and direct detection optical wireless communication system based on orthogonal frequency division multiplexing. The theory employs the Bussgang theorem, which is widely accepted as a means to characterise the impact of nonlinear distortions on normally-distributed signals. The current work proposes a new method to generalise this approach, and it describes how a closed-form analytical expression for the system bit error rate can be obtained for an arbitrary memoryless distortion. Major distortion effects at the transmitter stage such as quantisation and nonlinearity from the light-emitting-diode are analysed. Four known orthogonal-frequency-division-multiplexing-based modulation schemes for optical communication are considered in this study: direct-current-biased optical OFDM, asymmetrically clipped optical OFDM, pulse-amplitude-modulated discrete multitone modulation, and unipolar orthogonal frequency division multiplexing.**

***Index Terms*—Wireless communication, nonlinear distortion, OFDM, optical modulation.**

I. Introduction

WIRELESS data rates have been growing exponentially in the past decade. According to some recent forecasts, in 2015 more than 6 Exabytes of wireless data would be required per month [1]. The continuously enhanced wireless communication standards will not be able to fully satisfy the future demand for mobile data throughput because the available radio frequency (RF) spectrum is very limited. Hence, an expansion of the wireless spectrum into a new and largely unexplored domain – the visible light spectrum – has the potential to change the face of future wireless communications. The advantages of an optical wireless system include among others: 1) vast amount of unused bandwidth; 2) no licensing fees; 3) low-cost front end devices; and 4) no interference with sensitive electronic systems. In addition, the existing lighting infrastructure can be used for the realisation of visible light communication (VLC).

Optical wireless communication (OWC) using incoherent off-the-shelf illumination devices, which are the foremost candidates for mass-produced front-end elements, is realisable as an intensity modulation and direct detection (IM/DD) system. This means that only signal intensity can be detected reliably. Hence, without modification it is not possible to use all digital modulation techniques known in RF communication. Unipolar techniques like on-off keying (OOK), pulse-position modulation (PPM), and pulse-amplitude modulation (M-PAM) can be adopted in a relatively straightforward way. As transmission rates increase, however, unwanted intersymbol interference (ISI) appears. Hence, more resilient techniques such as orthogonal frequency division multiplexing (OFDM) are preferred. OFDM allows equalisation to be performed with single-tap equalisers in the frequency domain, which reduces design complexity and equalisation cost. It also allows different frequency subcarriers to be adaptively loaded with information according to the channel characteristics. This enables more optimal usage of the channel, especially when attenuation or interference is significant in certain frequency bands [2]. Conventional OFDM signals are bipolar and complex-valued. However, they have to be both real and unipolar in IM/DD systems. It is possible to transform an OFDM signal into a real signal by imposing Hermitian symmetry on the subcarriers in the frequency domain. Furthermore, a number of possible approaches to deal with the issue of bipolarity in OFDM signals have been proposed. The current work focuses on four of them, in particular: direct-current-biased optical OFDM (DCO-OFDM), asymmetrically clipped optical OFDM (ACO-OFDM) [3], pulse-amplitude-modulated discrete multitone modulation (PAM-DMT) [4], and unipolar orthogonal frequency division multiplexing (U-OFDM) [5]. It analytically characterises their performance in a nonlinear additive white Gaussian noise (AWGN) channel which is typical for an OWC system. Some of the schemes - DCO-OFDM and ACO-OFDM - have already been analysed in the context of certain nonlinearities that are present in OWC [6]–[10]. The current work gives a more complete analysis encompassing the joint effect of a number of different distortions which to the best of the authors' knowledge have not been analysed jointly in OWC and have never been analysed for PAM-DMT and U-OFDM. An interesting observation is that the concepts presented for U-OFDM have been previously introduced in Flip-OFDM [11]. In addition, the four schemes, ACO-OFDM, PAM-DMT, U-OFDM and Flip-OFDM, perform equivalently in a simple AWGN channel [3]–[5], [11].

An information signal in an OWC system undergoes a number of distortions, including nonlinear ones. Linear distortions such as attenuation and ISI can be compensated with amplifiers, equalisers and signal processing. Nonlinear distortions, however, often make irreversible changes to the signal. Therefore, it is necessary to be able to characterise

Manuscript received September 01, 2012; revised February 01, 2013 and June 04, 2013; accepted July 30, 2013.

The authors gratefully acknowledge support for this work from the UK Engineering and Physical Sciences Research Council (EPSRC) under grant EP/I013539/1.

D. Tsonev and H. Haas are with The University of Edinburgh, Edinburgh, EH9 3JL, UK, (e–mail: {d.tsonev, h.haas}@ed.ac.uk.).

S. Sinanovic is with Glasgow Caledonian University, Glasgow, G4 0BA, UK, (e–mail: sinan.sinanovic@gcu.ac.uk).

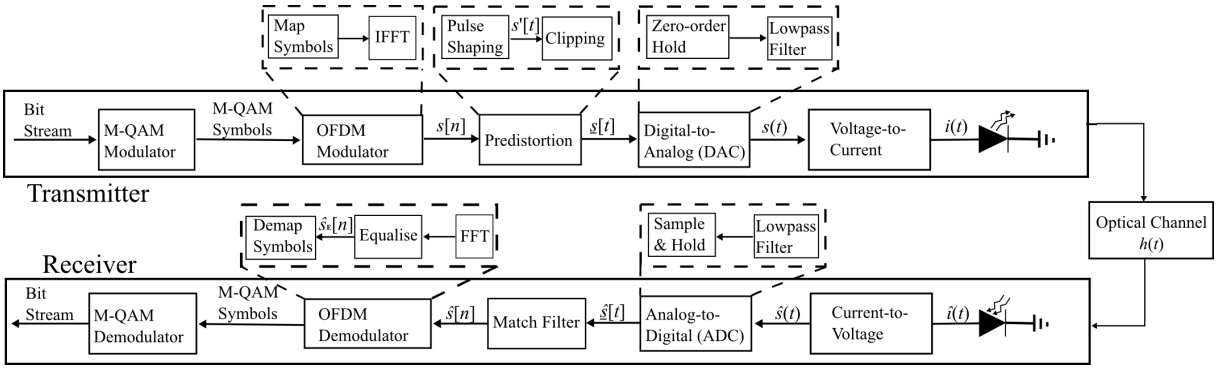

Fig. 1. Optical Wireless Communication System

and evaluate distortion effects as fully as possible. Such examples include quantisation effects in the digital-to-analog converters (DACs) and analog-to-digital converters (ADCs), as well as the effects caused by the nonlinear output characteristic of a light emitting diode (LED). A number of works have been published on distortion in OFDM-based modulation schemes [6]–[10], [12]–[16]. A significant number of them focus specifically on the nonlinear distortions present in an OWC system [6]–[10]. The analysis of nonlinear distortion is not straightforward. Even though general procedures have been introduced for obtaining an analytical solution [12], a closed-form solution is not always available. The current work describes a complete general procedure which *always* leads to a closed-form solution. It can be used to solve the problems presented in [6]–[10] as well as to analyse any other arbitrary memoryless nonlinear distortion, which can be part of an OWC system based on OFDM. The specific case study in this paper involves a complete set of the significant nonlinear effects at the transmitter combining distortion due to quantisation at the DAC as well as distortion due to the nonlinear characteristic of the LED. Pulse shaping has also been considered unlike in previous works on the subject [6]–[10].

The rest of this paper is organised as follows. Section II provides a description of the OWC system. Section III describes the modulation schemes under investigation. Section IV discusses the issues incurred by pulse shaping techniques in IM/DD transmission systems. Section V introduces the expected nonlinearities in an OWC system. Section VI presents the theoretical approach for obtaining a closed-form assessment of the performance. Section VII confirms analytical solutions with numerical simulations. Finally, section VIII provides concluding remarks.

II. OWC System

The diagram of an OWC system is presented in Fig. 1. The incoming bits are divided into data chunks and mapped to symbols from a known modulation scheme such as quadrature amplitude modulation (M-QAM) or M-PAM. The M-QAM/M-PAM symbols are modulated onto different frequency subcarriers according to one of the following schemes: DCO-OFDM, ACO-OFDM, PAM-DMT, U-OFDM. Then, the resulting time domain signal is subjected to a number of predistortion techniques, which condition it for transmission. This block includes oversampling, pulse shaping as well as clipping any values below the allowed minimum or above the allowed maximum. Clipping is performed because a DAC, an amplifier, and an LED can only operate in a limited range, specified by their electrical properties. The conditioned signal is fed to a DAC which outputs an analog signal. This stage of the system consists of a zero-order-hold element or other type of interpolator followed by a low pass filter. The output signal from the zero-order hold is continuous in time. However, because the signal has discrete amplitude levels, corresponding to the samples of the oversampled pulse-shaped and clipped signal $s'[t]$, it is analysed in terms of the discrete time-domain signal $s'[t]$. It is assumed that the oversampling is sufficient, and the pulse shaping operation is such that the low-pass filter after the zero-order hold outputs a continuous-time signal which is equivalent to the signal at its input for all practical considerations. Hence, in the analysis, nonlinear transformations of the signal $s'[t]$ are investigated. The analog output of the DAC is encoded into a current signal by a voltage-to-current transducer with appropriate bias and supplied to the LED. OFDM-based OWC with incoherent off-the-shelf illumination devices can only be realised as a baseband communication technique. Therefore, frequency upconversion is not required and, thus, has not been considered in the presented analysis. Light intensity at the diode varies with the current. At the receiver side, a photo diode transforms the variations in the intensity of the received light into variations of a current signal, which is turned into a voltage signal by a transimpedance amplifier. The resulting signal is discretised at an ADC and passed on to the processing circuitry, which includes a matched filter, an OFDM demodulator with an equaliser, as well as a bit demodulator.

III. OFDM Modulation Schemes

The modulation schemes presented in this paper are modifications of conventional OFDM. The subcarriers in the frequency domain are modulated with M-QAM symbols in the case of DCO-OFDM, ACO-OFDM, and U-OFDM and with M-PAM symbols in the case of PAM-DMT. A time-domain block of samples is obtained by taking the inverse fast Fourier transform (IFFT) of a block of N_{FFT} complex M-QAM/M-PAM symbols. Hermitian symmetry is imposed, which, according to the properties of the Fourier transform, generates a real time-domain signal [17]. The subcarriers at positions $k{=}0$ and $k{=}\frac{N_{\mathrm{FFT}}}{2}$ are set to zero in order to satisfy

the requirements of the Hermitian symmetry. The real time-domain signal is bipolar in nature. An LED can convey only positive signals when it is active. Hence, the following four different methods have been designed for the generation of unipolar signals, suitable for OWC.

A. DCO-OFDM

DCO-OFDM generates a unipolar signal by introducing a DC bias. Fig. 2 illustrates the concept. The spectral efficiency of the scheme is:

$$\eta_{\mathrm{DCO}} = \frac{\log_2(M)(N_{\mathrm{FFT}}-2)}{2(N_{\mathrm{FFT}}+N_{\mathrm{cp}})} \ \text{bits/s/Hz} \tag{1}$$

provided that all available carriers are loaded with M-QAM. The factors $N_{\mathrm{FFT}}-2$ and 0.5 occur due to the Hermitian symmetry requirement. N_{cp} is the length of the cyclic prefix.

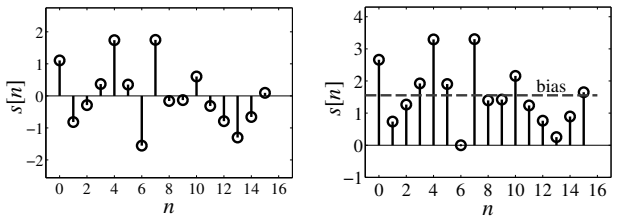

(a) Bipolar OFDM before biasing. (b) Biased DCO-OFDM.

Fig. 2. DCO-OFDM Generation. Cyclic prefix is not illustrated.

OFDM has a very high peak-to-average power ratio (PAPR). Following the calculations presented in [18], a lower bound for the PAPR of real signals can be calculated as follows:

$$\frac{3N_{\mathrm{a}}(\sqrt{M}-1)}{2\sqrt{M}+1} \tag{2}$$

where N_{a} is the number of modulated carriers in the frequency domain. Therefore, it is impractical to introduce a biasing level which ensures that all possible time samples are positive. In addition, electronic elements have an operational range, which is limited both in terms of a minimum and a maximum value. Hence, an OFDM signal would be clipped both from above and from below in order to fit within the required range. A typical value of a few signal standard deviations is used in practice for clipping on each side of the signal distribution. This distortion is easily modeled by the upper and lower limit of the DAC. This modeling approach is adopted in the current study.

B. ACO-OFDM

Biasing in DCO-OFDM increases the dissipated electrical and optical energy at the transmitter by a substantial amount. The dissipated electrical energy is proportional to $\mathrm{E}[i^2(t)] = \mathrm{E}[(i_{\mathrm{signal}}(t)+i_{\mathrm{bias}}(t))^2]$, and the dissipated optical energy is proportional to $\mathrm{E}[i(t)] = \mathrm{E}[i_{\mathrm{signal}}(t)+i_{\mathrm{bias}}(t)]$, where $E[\cdot]$ denotes statistical expectation. ACO-OFDM, illustrated in Fig. 3, avoids the biasing requirement of DCO-OFDM by exploiting the properties of the Fourier transform so that a unipolar signal can be generated without biasing. As presented in [3], only odd frequency subcarriers are modulated. This creates a symmetry between samples in the time-domain OFDM frame. In general, if $s(k,n)$ is the contribution of subcarrier $S[k]$ to the sample at time n, then [3]:

$$\begin{aligned} s(k,n) &= \frac{1}{\sqrt{N_{\mathrm{FFT}}}} S[k] e^{\frac{j2\pi nk}{N_{\mathrm{FFT}}}} \\ s(k,n+\frac{N_{\mathrm{FFT}}}{2}) &= \frac{1}{\sqrt{N_{\mathrm{FFT}}}} S[k] e^{\frac{j2\pi(n+N_{\mathrm{FFT}}/2)k}{N_{\mathrm{FFT}}}} = \\ &= \frac{1}{\sqrt{N_{\mathrm{FFT}}}} S[k] e^{\frac{j2\pi nk}{N_{\mathrm{FFT}}}} e^{j\pi k}. \end{aligned} \tag{3}$$

For odd values of k, $s(k,n) = -s(k,n+N_{\mathrm{FFT}}/2)$. For even values of k, $s(k,n) = s(k,n+N_{\mathrm{FFT}}/2)$. Hence, if only the odd subcarriers in an OFDM frame are modulated, the time-domain signal, $s[n]$, has the property:

$$s[n] = -s[n+N_{\mathrm{FFT}}/2]. \tag{4}$$

If only the even subcarriers in an OFDM frame are modulated, the time-domain signal has the property:

$$s[n] = s[n+N_{\mathrm{FFT}}/2]. \tag{5}$$

Because complex exponential functions are orthogonal to each other, if a signal has the property in (4), this means that in the frequency domain only odd samples contain information. Similarly, if a signal has the property in (5), then in the frequency domain only its even samples contain information. Clipping the negative samples of an arbitrary time-domain signal, $s[n]$, can be represented as:

$$\mathrm{CLIP}(s[n]) = \frac{1}{2}(s[n]+|s[n]|). \tag{6}$$

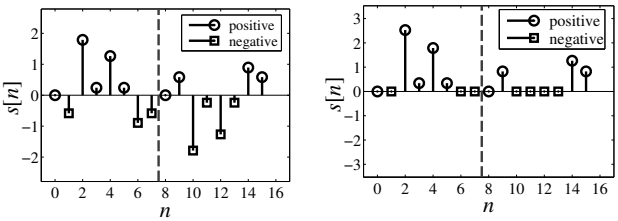

(a) ACO-OFDM before clipping. (b) ACO-OFDM after clipping.

Fig. 3. ACO-OFDM Generation. Cyclic prefix is not illustrated.

In ACO-OFDM, only the odd subcarriers are modulated. Hence, (4) applies. Therefore, $s[n] = -s[n+N_{\mathrm{FFT}}/2]$. Then $|s[n]| = |s[n+N_{\mathrm{FFT}}/2]|$. This symmetry allows all negative values to be removed. The clipping distortion $|s[n]|$, described in (6), has the property stipulated in (5), and so it distorts only the even subcarriers. The factor 0.5 occurs from the clipping and is consistent with the analysis presented in [3]. An additional factor of $\sqrt{2}$ is introduced to rescale the unipolar signal and normalise the amount of dissipated energy, which would lead to an overall signal-to-noise ratio (SNR) performance penalty of 3dB. This short proof describes the analysis in [3] in a more concise manner. Not using the even subcarriers sacrifices about half the spectral efficiency, compared to DCO-OFDM, and it becomes:

$$\eta_{\mathrm{ACO}} = \frac{\log_2(M)N_{\mathrm{FFT}}}{4(N_{\mathrm{FFT}}+N_{\mathrm{cp}})} \ \text{bits/s/Hz}. \tag{7}$$

C. PAM-DMT

In PAM-DMT, illustrated in Fig. 4, the frequency subcarriers in an OFDM frame are modulated with imaginary symbols from the M-PAM modulation scheme. Due to Hermitian symmetry in the frequency domain, the PAM-DMT time-domain signal becomes [4]:

$$s[n] = \frac{1}{\sqrt{N_{\mathrm{FFT}}}} \sum_{k=0}^{N_{\mathrm{fft}}-1} S[k] e^{\frac{j2\pi kn}{N_{\mathrm{FFT}}}} = \tag{8}$$

$$= \frac{1}{\sqrt{N_{\mathrm{FFT}}}} \sum_{k=0}^{N_{\mathrm{FFT}}-1} S[k] \left(\cos \frac{2\pi kn}{N_{\mathrm{FFT}}} + j \sin \frac{2\pi kn}{N_{\mathrm{FFT}}} \right) =$$

$$= \frac{1}{\sqrt{N_{\mathrm{FFT}}}} \sum_{k=0}^{N_{\mathrm{FFT}}-1} jS[k] \sin \frac{2\pi kn}{N_{\mathrm{FFT}}}. \tag{9}$$

The time-domain structure of a PAM-DMT frame exhibits an antisymmetry where $s[0]{=}0$, $s[N_{\mathrm{FFT}}/2]{=}0$ if N_{FFT} is even, and $s[n]{=}-s[N_{\mathrm{FFT}}-n]$. This means that $|s[0]|{=}0$, $|s[N_{\mathrm{FFT}}/2]|{=}0$ if N_{FFT} is even, and $|s[n]|{=}|s[N_{\mathrm{FFT}}-n]|$. Therefore, if the negative values are removed, as described in (6), the distortion term $|s[n]|$ has Hermitian symmetry in the time domain. This means that in the frequency domain, the distortion is transformed into a real-valued signal. Hence, it is completely orthogonal to the useful information. This proof has not been formally completed in [4], but it is straightforward with the representation of clipping in (6). The spectral efficiency of PAM-DMT is:

$$\eta_{\mathrm{PAM-DMT}} = \frac{\log_2(M)(N_{\mathrm{FFT}}-2)}{2(N_{\mathrm{FFT}}+N_{\mathrm{cp}})} \ \mathrm{bits/s/Hz} \tag{10}$$

where M denotes the order of M-PAM modulation. It should be noted that $\sqrt{M}$-PAM has roughly the same performance as M-QAM in an AWGN channel. This makes PAM-DMT comparable to ACO-OFDM in spectral efficiency for the same bit error rate (BER) performance.

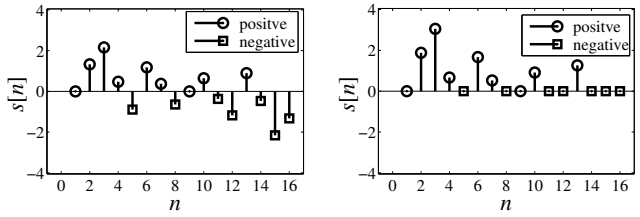

(a) Bipolar PAM-DMT before clipping. (b) Unipolar PAM-DMT after clipping and rescale.

Fig. 4. PAM-DMT Generation. Cyclic prefix is not illustrated.

D. U-OFDM

In U-OFDM, all possible subcarriers in the frequency domain are modulated as in DCO-OFDM. After the time-domain signal is obtained, it is divided into two blocks: a positive and a negative one. The positive block is a copy of the original signal frame, where all negative samples are set to zero. The negative block is a copy of the original signal frame, where all samples are multiplied by -1 to switch signs. After this operation, the negative samples are set to zero. The principle of how both blocks form the original OFDM frame can be observed in Fig. 5(a). The two blocks are transmitted separately. This can be seen in Fig. 5(b). The cyclic prefixes are omitted in the given examples for simplicity of illustration. The increased number of samples in the time domain decreases the spectral efficiency by a factor of 0.5 compared to DCO-OFDM, and it becomes:

$$\eta_{\mathrm{U}} = \frac{\log_2(M)(N_{\mathrm{FFT}}-2)}{4(N_{\mathrm{FFT}}+N_{\mathrm{cp}})} \ \mathrm{bits/s/Hz}. \tag{11}$$

At the demodulator, the original OFDM frame is obtained by subtracting the negative block from the positive one. This effectively doubles the noise at each resulting sample, and so the performance of U-OFDM becomes the same as the performance of ACO-OFDM and PAM-DMT where the clipping introduces an SNR penalty of 3 dB.

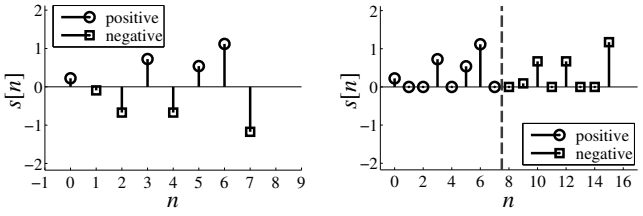

(a) Bipolar OFDM. (b) Unipolar U-OFDM.

Fig. 5. U-OFDM Generation. Cyclic prefixes are not illustrated.

IV. Pulse Shaping

An LED is modulated with a continuous electrical signal, and it emits a continuously varying light signal. A digital implementation of OFDM generates discrete values which need to be encoded into an analog signal, suitable to modulate the LED. The pulse shaping operation allows digital samples to be mapped to continuous pulse shapes. The selection of the pulse-shaping filters is important because the communication channel restricts the bandwidth of the signals which can be successfully propagated to the receiver. The maximum modulation frequency of off-the-shelf white LEDs is in the order of 2 MHz and in the order of 20 MHz when blue filering is applied at the receiver [19]. The transmitted information signals must be tailored to fit in that frequency range in order to avoid distortion. Different pulse shapes have different time-domain properties as well as different bandwidth requirements. An example of a pulse shape is a square pulse which corresponds to the zero-order hold function of a DAC [20]. This shape is easy to implement and has a time duration which is perfectly limited within a symbol period. However, it requires an infinite bandwidth. Therefore, it is not possible to realise it without distorting the received signal. In practice, if square pulses are used as an interpolation technique, the signal is low-pass-filtered afterwards to incorporate only a desired portion of the frequencies, for example, until the first zero crossing in the frequency domain. This occurs at $1/T_{\mathrm{s}}$ if T_{s} is the symbol period. A similar shape is the triangle pulse, which corresponds to a first-order interpolation of discrete samples [20]. This shape is characterised with an improved bandwidth profile and a longer time-domain duration compared to the square pulse. Exact recovery of the transmitted signal, without ISI, requires accurate sampling at the receiver. Theoretically, the most bandwidth efficient interpolation filter is the sinc

function [20]. Its bandwidth requirement is $1/2T_{\rm s}$, so it is two times more efficient than a square pulse low-pass-filtered at the first zero crossing. However, it spans an impulse response with an infinite duration in the time domain. This means that in practice the shape is truncated, and due to the longer impulse response, it requires more processing. In addition, time jitter can introduce significant ISI. For this reason, the raised-cosine filter and its modified version, the root-raised cosine filter, are used in many practical implementations. They allow the generation of an interpolation pulse with an arbitrary bandwidth requirement between $1/2T_{\rm s}$ and $1/T_{\rm s}$ dependent on an adjustable roll-off factor. The raised cosine filter gives the designer the freedom to choose between the length of the pulse in the time domain and the frequency requirement of the shape. In practice, these filters are implemented by oversampling the discrete signal, interpolating it with a discrete pulse shape and then supplying it to the DAC, which typically consists of a zero-order hold and a low-pass filter as described in Fig. 1.

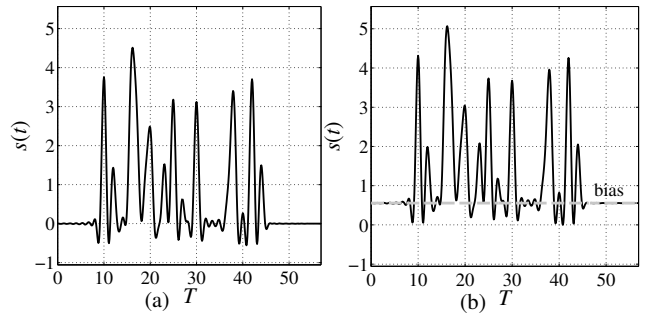

Fig. 6. (a) ACO-OFDM pulse-shaped after removing negative values. (b) Addition of necessary bias to make the pulse-shaped signal unipolar.

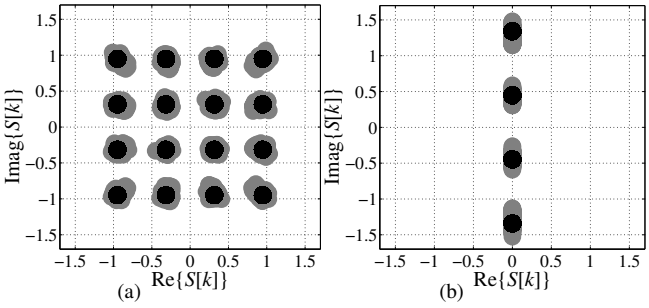

Fig. 7. (a) Distortion in ACO-OFDM/U-OFDM after clipping negative values of the pulse-shaped unipolar signal. (b) Distortion in PAM-DMT after clipping negative values of the pulse-shaped unipolar signal.

Signals in ACO-OFDM, PAM-DMT, and U-OFDM are made unipolar after clipping of the negative values. Bipolar pulse shapes like the sinc and the raised-cosine filter turn a *unipolar* signal before pulse shaping into a *bipolar* signal after pulse shaping. An example is presented in Fig. 6. The issue can be solved by introducing a bias to account for the negative values. This leads to an increase in the energy consumption of approximately 3 dB. Alternatively, the negative values after pulse shaping can be clipped at zero again, but this leads to the distortion presented in Fig. 7. Therefore, it is important to implement pulse shaping before the negative values in ACO-OFDM, PAM-DMT, and U-OFDM are removed. Then, as described in (6), the clipping operation leads to a unipolar signal that consists of the original bipolar signal and a distortion term which is present both inside and outside the desired bandwidth. The useful signal, however, remains within the bandwidth limit and is not affected by the distortion term as described in Section III. The rest of this section provides a proof.

The sampling frequency is denoted by $F_{\rm s}$, $T_{\rm s}$ denotes the symbol period, $T{=}F_{\rm s}T_{\rm s}$ denotes the discrete-time symbol period, and $p[t]$ denotes the digital pulse shape. Then, the part of the oversampled pulse-shaped discrete bipolar signal, which contains the information of a given frame, is expressed as:

$$s'[t] = \sum_{n=N_{\rm FFT}-N_{\rm cp}}^{N_{\rm FFT}-1} s[n,0]p[t{-}(n{-}N_{\rm FFT})T] + \sum_{n=0}^{N_{\rm FFT}-1} s[n,0]p[t{-}nT] + \sum_{n=N_{\rm FFT}-N_{\rm cp}}^{N_{\rm FFT}-N_{\rm cp}+N_{\rm cp}^{\rm p}-1} s[n,1]p[t{-}(N_{\rm FFT}{+}N_{\rm cp})T{-}(n-N_{\rm FFT})T] \tag{12}$$

where $N_{\rm cp}^{\rm p}$ is the length of the cyclic prefix sufficient to remove the effects of $p[t]$, and $s[n,0]$ indicates the nth sample of the OFDM frame at position 0, *i.e.*, the current frame. The discrete-time pulse-shaped bipolar signal relevant for sampling the first $\frac{N_{\rm FFT}}{2}$ points of the current frame can be expressed as:

$$s'_1[t] = \sum_{n=N_{\rm FFT}-N_{\rm cp}}^{N_{\rm FFT}-1} s[n,0]p[t{-}(n{-}N_{\rm FFT})T] + \sum_{n=0}^{N_{\rm FFT}/2-1} s[n,0]p[t{-}nT] + \sum_{n=N_{\rm FFT}/2}^{N_{\rm FFT}/2-1+N_{\rm cp}^{\rm p}} s[n,0]p[t{-}nT]. \tag{13}$$

The discrete-time pulse-shaped bipolar signal relevant for sampling the next $\frac{N_{\rm FFT}}{2}$ points of the current frame can be expressed as:

$$s'_2[t] = \sum_{n=N_{\rm FFT}/2-N_{\rm cp}}^{N_{\rm FFT}/2-1} s[n,0]p[t{-}nT] + \sum_{n=N_{\rm FFT}/2}^{N_{\rm FFT}-1} s[n,0]p[t{-}nT] + \sum_{n=N_{\rm FFT}-N_{\rm cp}}^{N_{\rm FFT}-N_{\rm cp}+N_{\rm cp}^{\rm p}-1} s[n,1]p[t{-}(N_{\rm FFT}{+}N_{\rm cp})T{-}(n-N_{\rm FFT})T]. \tag{14}$$

The discrete-time unipolar signal, ready for digital-to-analog conversion and transmission, can be expressed as:

$$\underline{s}[t] = \sqrt{2}\mathrm{CLIP}\left(s'[t]\right) = \frac{1}{\sqrt{2}}\left(s'[t] + |s'[t]|\right). \tag{15}$$

At the receiver, the samples of a given frame after match filtering can be expressed as:

$$\begin{aligned}\hat{s}[n] &= \left(\underline{s}[t] * h[t] + n[t]\right) * p[t]\big|_{t=nT} \\ &= \left(\frac{1}{\sqrt{2}}\left(s'[t] + |s'[t]|\right) * h[t] + n[t]\right) * p[t]\Big|_{t=nT} \\ &= \begin{cases}\left(\frac{1}{\sqrt{2}}\left(s_1'[t]+|s_1'[t]|\right) * h[t]+n[t]\right) * p[t]\Big|_{t=nT}, & n < \frac{N_{\rm FFT}}{2} \\ \left(\frac{1}{\sqrt{2}}\left(s_2'[t]+|s_2'[t]|\right) * h[t]+n[t]\right) * p[t]\Big|_{t=nT}, & \frac{N_{\rm FFT}}{2} \le n\end{cases}\end{aligned} \tag{16}$$

where $*$ denotes convolution, $n[t]$ denotes AWGN, and $h[t]$ denotes the impulse response of the channel in discrete time. The cyclic prefix is sufficient to remove ISI and to turn the *continuous*-time convolution with the channel, $h(t)$, into a circular convolution in *discrete* time with the channel, $h[t]$. Assuming perfect channel knowledge, the equalised samples at the receiver are expressed as:

$$\begin{aligned}\hat{s}_{\mathrm{E}}[n] &= \left(\underline{s}[t] + n[t] * h^{-1}[t]\right) * p[t]\Big|_{t=nT} \\ &= \left(\frac{1}{\sqrt{2}}\left(s'[t] + |s'[t]|\right) + n[t] * h^{-1}[t]\right) * p[t]\Bigg|_{t=nT} \\ &= \begin{cases} \left(\frac{1}{\sqrt{2}}\left(s_1{}'[t] + |s_1{}'[t]|\right) + n[t] * h^{-1}[t]\right) * p[t]\Big|_{t=nT}, & n < \frac{N_{\mathrm{FFT}}}{2} \\ \left(\frac{1}{\sqrt{2}}\left(s_2{}'[t] + |s_2{}'[t]|\right) + n[t] * h^{-1}[t]\right) * p[t]\Big|_{t=nT}, & \frac{N_{\mathrm{FFT}}}{2} \leq n. \end{cases}\end{aligned} \tag{17}$$

A. ACO-OFDM

In ACO-OFDM, $s[n] = -s[n + N_{\mathrm{FFT}}/2]$. Therefore, ${s'}_1[t] \approx -{s'}_2[t + \frac{N_{\mathrm{FFT}}}{2}T]$ except for the third terms in (13) and (14). Differences appear because in the time domain $p[t]$ spans beyond a single symbol duration and beyond the boundaries of the OFDM frame. However, this effect is not significant when $N_{\mathrm{cp}}^{\mathrm{p}} << N_{\mathrm{FFT}}$. As a consequence, $|{s'}_1[t]| \approx \left|{s'}_2[t + \frac{N_{\mathrm{FFT}}}{2}T]\right|$. At the receiver, the distortion term in the first $\frac{N_{\mathrm{FFT}}}{2}$ points, $\frac{1}{\sqrt{2}}|{s'}_1[t]| * h[t] * p[t]\Big|_{nT}$, is the same as the distortion term in the second $\frac{N_{\mathrm{FFT}}}{2}$ points, $\frac{1}{\sqrt{2}}|{s'}_2[t]| * h[t] * p[t]\Big|_{nT}$, because $|{s'}_1[t]| \approx \left|{s'}_2\left[t + \frac{N_{\mathrm{FFT}}}{2}T\right]\right|$. Therefore, distortion falls on the even subcarriers only as described in Section III-B.

B. PAM-DMT

In PAM-DMT, $s[n] = -s[N_{\mathrm{FFT}} - n]$. Therefore, with the representations in (13) and (14), ${s'}_1[t] \approx -{s'}_2[N_{\mathrm{FFT}}T - t]$. Again, differences appear between the first term in (13) and the third term in (14). The differences are caused by the time-domain span of $p[t]$ but are not significant for $N_{\mathrm{cp}}^{\mathrm{p}} << N_{\mathrm{FFT}}$. Hence, it can be concluded that $|{s'}_1[t]| \approx |{s'}_2[N_{\mathrm{FFT}}T - t]|$. The pulse-shaping filter's impulse response is an even function, so $p[t] = p[-t]$. From (17), the distortion term after equalisation consists of $\frac{1}{\sqrt{2}}|{s'}_1[t]| * p[t]\Big|_{t=nT}$ and $\frac{1}{\sqrt{2}}|{s'}_2[t]| * p[t]\Big|_{t=nT}$. It maintains Hermitian symmetry, and hence noise due to distortion is orthogonal to useful information as described before in Section III-C.

C. U-OFDM

The U-OFDM bipolar *discrete* signal is encoded in two consecutive frame blocks. The oversampled discrete-time bipolar part of $s'[t]$ which contains the information of the positive frame block can be expressed with the representation in (12) and denoted as ${s'}^{\mathrm{p}}[t]$. The oversampled discrete-time bipolar part of $s'[t]$ which contains the information of the negative frame block can be expressed with the representation in (12) and denoted as ${s'}^{\mathrm{n}}[t]$. If $s^{\mathrm{p}}[n]$ denotes the original bipolar samples of the positive frame block, and $s^{\mathrm{n}}[n]$ denotes the original bipolar samples of the negative frame block, then by design $s^{\mathrm{p}}[n] = -s^{\mathrm{n}}[n]$. Hence, a closer look at (12) shows that ${s'}^{\mathrm{p}}[t] = -{s'}^{\mathrm{n}}[t]$ except for the third terms in the summation. The differences appear due to the time-domain span of $p[t]$ but are not significant when $N_{\mathrm{cp}}^{\mathrm{p}} << N_{\mathrm{FFT}}$. Then, the samples of the positive frame block and the negative frame block after match filtering at the receiver become respectively:

$$\hat{s}^{\mathrm{p}}[n] = \left(\frac{1}{2}\left({s'}^{\mathrm{p}}[t] + |{s'}^{\mathrm{p}}[t]|\right) * h[t] + n_1[t]\right) * p[t]\Big|_{t=nT} \tag{18}$$

$$\hat{s}^{\mathrm{n}}[n] = \left(\frac{1}{2}\left({s'}^{\mathrm{n}}[t] + |{s'}^{\mathrm{n}}[t]|\right) * h[t] + n_2[t]\right) * p[t]\Big|_{t=nT} \tag{19}$$

where $n_1[t]$ and $n_2[t]$ are two independent identically-distributed instances of the AWGN process. The bipolar samples at the receiver can be reconstructed by subtracting the received samples of the negative frame block from the received samples of the positive frame block:

$$\begin{aligned}\hat{s}^{\mathrm{b}}[n] &= \hat{s}^{\mathrm{p}}[n] - \hat{s}^{\mathrm{n}}[n] \\ &= \left(\frac{1}{2}\left({s'}^{\mathrm{p}}[t] - {s'}^{\mathrm{n}}[t]\right) * h[t] + n_1[t] - n_2[t]\right) * p[t]\Big|_{t=nT}.\end{aligned} \tag{20}$$

The nonlinear distortion terms $\frac{1}{2}|{s'}^{\mathrm{p}}[t]| * h[t] * p[t]\Big|_{t=nT}$ and $\frac{1}{2}|{s'}^{\mathrm{n}}[t]| * h[t] * p[t]\Big|_{t=nT}$ are equal and so are completely removed by the subtraction operation. The noise doubles as described in Section III-D.

An important implication of these proofs is that pulse shaping can also be incorporated in the analysis of the nonlinear distortions for ACO-OFDM, PAM-DMT, and U-OFDM. If pulse shaping is applied after clipping at zero, then the distribution of samples in the time domain changes, and that compromises the accuracy of the analysis. OFDM samples in the time domain follow a Gaussian distribution when the number of carriers is greater than 64 [8], [10], [12]. Hence, the positive samples of ACO-OFDM, PAM-DMT, and U-OFDM follow the distribution of a Gaussian function, clipped at zero. Pulse shaping is a linear operation, which linearly combines the discrete samples of an OFDM frame, scaled by the samples of a pulse-shaping filter. Linearly combining samples that follow a clipped Gaussian distribution results in samples that follow a different distribution. Hence, pulse shaping after clipping at zero produces a signal which cannot be analysed with the Bussgang theorem. On the other hand, combining samples that follow a Gaussian distribution results in samples that again follow a Gaussian distribution. Hence, if the pulse shaping is done before the clipping at zero, the pulse-shaped samples follow a Gaussian distribution and after the clipping operation they follow a clipped Gaussian distribution. This enables the use of the Bussgang theorem and the analysis presented in this work.

V. Nonlinearities in OWC

There are a number of possible sources of nonlinear distortion in an OWC system. Electronic devices have limited dynamic ranges and often nonlinear characteristics within the

dynamic range. Furthermore, transitions between the digital and the analog domain lead to signal quantisation effects.

The processed digital time-domain signal needs to be passed through a DAC in order to obtain a signal, which can be used to drive the LED. An increase in the resolution of a DAC increases the design complexity and cost. Decreasing the resolution leads to signal quantisation. In addition, nonlinear distortion occurs from the limited range of the device which leads to clipping. An accurate analysis of the distortion effects caused to a signal allows for making informed choices between cost, range and accuracy of the DAC.

LEDs and photodiodes (PDs) are another source of nonlinearity. The voltage-current relationship at an LED is not linear. With the design of suitable V-to-I transducers, this transition step in the system can be almost completely linearised. However, the relationship between the current through the LED and the produced light intensity is also not linear. In addition, there is a minimum and a maximum allowed current level so that the diode can operate properly. This means that the OFDM signal should be clipped at the processing step in order to become suitable for transmission through the LED. The same effects due to the nonlinear relationships between light intensity, current and voltage are present in the PD. However, this device operates in a much smaller range, which means that distortion is not as significant as in the LED.

VI. Nonlinearity Analysis

For a large number of subcarriers, $N_{\text{FFT}} > 64$, an OFDM time-domain signal can be approximated by a set of independent identically distributed random variables with a continuous Gaussian distribution [8], [10], [12]. According to [12], a nonlinear distortion in an OFDM-based system can be described with a gain factor and an additional noise component, both of which can be explained and quantified with the help of the Bussgang theorem. If X is a zero-mean Gaussian random variable and $\mathrm{z}(X)$ is an arbitrary memoryless distortion on X, then following the Bussgang theorem in [21] and Rowe's subsequent work in [22],

$$\mathrm{z}(X) = \alpha X + Y \tag{21}$$

$$\mathrm{E}[XY] = 0. \tag{22}$$

In these equations, α is a constant, $\mathrm{E}[\cdot]$ stands for statistical expectation, and Y is a noise component not correlated with X. Using (21) and (22), α can be derived as:

$$\alpha = \frac{\mathrm{E}[X\mathrm{z}(X)]}{\sigma_{\mathrm{x}}^2} \tag{23}$$

where σ_{x} is the standard deviation of X. The noise component Y can be quantified as follows:

$$\mathrm{E}[Y^2] = \mathrm{E}[\mathrm{z}^2(X)] - \alpha^2\sigma_{\mathrm{x}}^2 \tag{24}$$

$$\mathrm{E}[Y] = \mathrm{E}[\mathrm{z}(X)] \tag{25}$$

$$\sigma_{\mathrm{Y}}^2 = \mathrm{E}[Y^2] - \mathrm{E}[Y]^2 \tag{26}$$

where σ_{Y}^2 denotes the variance of Y. When the fast Fourier transform (FFT) is applied at the system receiver, in the frequency domain the noise Y is transformed into additive Gaussian noise due to the central limit theorem (CLT). The variance of Y in the frequency domain is again σ_{Y}^2, and its time-domain average contributes only to the 0th subcarrier. Therefore, at each modulated subcarrier an additional zero-mean additive Gaussian noise component with variance σ_{Y}^2 is present. Overall the system experiences an increase in the additive Gaussian noise power by σ_{Y}^2 and a decrease in the useful signal power by a factor of α^2. This approach has been used in a number of works to analyse nonlinearities in an analytical or semi-analytical fashion [8], [10], [12]. The analytical solution, however, is not guaranteed to be in a closed form. Whenever a closed-form solution is desired, an additional step is required as the derivation needs to be tailored to the respective nonlinear distortion function. In the current paper, a general derivation approach which leads to a closed-form analytical solution with arbitrary accuracy for an arbitrary memoryless distortion function is proposed. It is applicable to the four OFDM-based modulation schemes investigated in this work. The rest of this section introduces the modified technique and describes how it can be applied to DCO-OFDM, ACO-OFDM, PAM-DMT, and U-OFDM.

An arbitrary distortion function $\mathrm{z}(X)$ can be expressed as a set of intervals I with cardinality $|I|$ and a set of continuous polynomials which accurately approximate $\mathrm{z}(X)$ in those intervals. The polynomials can be generated through interpolation of empirical data, or with a polynomial expansion of a function. The polynomial degree sets the accuracy of the approximation. Then $\mathrm{z}(x)$ can be represented as:

$$\mathrm{z}(x) = \sum_{l=1}^{|I|}\sum_{j=0}^{n_l} c_{l,j}x^j\left(\mathrm{U}(x - x_{\min,l}) - \mathrm{U}(x - x_{\max,l})\right) \tag{27}$$

where l denotes the lth interval, n_l denotes the order of the polynomial in interval l, $c_{l,j}$ denotes the jth polynomial coefficient in interval l, and $\mathrm{U}(x)$ is the unit step function. Moreover, $x_{\min,l}$ and $x_{\max,l}$ denote the lower and upper boundaries of interval l. Then α can be calculated as:

$$\begin{aligned}
\alpha &= \frac{\mathrm{E}[X\mathrm{z}(X)]}{\sigma_{\mathrm{x}}^2} = \frac{1}{\sigma_{\mathrm{x}}^2}\int_{-\infty}^{\infty} x\mathrm{z}(x)\frac{1}{\sigma_{\mathrm{x}}}\phi\left(\frac{x}{\sigma_{\mathrm{x}}}\right)\mathrm{d}x \\
&= \frac{1}{\sigma_{\mathrm{x}}^2}\int_{-\infty}^{\infty}\left\{\sum_{l=1}^{|I|}\sum_{j=0}^{n_l} c_{l,j}x^{j+1}\left(\mathrm{U}(x - x_{\min,l})\right.\right. \\
&\quad \left.\left. -\mathrm{U}(x - x_{\max,l})\right)\right\}\frac{1}{\sigma_{\mathrm{x}}}\phi\left(\frac{x}{\sigma_{\mathrm{x}}}\right)\mathrm{d}x \\
&= \frac{1}{\sigma_{\mathrm{x}}^2}\sum_{l=1}^{|I|}\sum_{j=0}^{n_l} c_{l,j}\int_{x_{\min,l}}^{x_{\max,l}} x^{j+1}\frac{1}{\sigma_{\mathrm{x}}}\phi\left(\frac{x}{\sigma_{\mathrm{x}}}\right)\mathrm{d}x \\
&\overset{(46)}{=} \frac{1}{\sigma_{\mathrm{x}}^2}\sum_{l=1}^{|I|}\sum_{j=0}^{n_l} c_{l,j}\left.\frac{\mathrm{d}^{j+1}\mathrm{D}(t, x_{\min,l}, x_{\max,l}, 0, \sigma_{\mathrm{x}})}{\mathrm{d}t^{j+1}}\right|_{t=0}
\end{aligned} \tag{28}$$

where function $\mathrm{D}(t, a, b, \mu, \sigma_{\mathrm{x}})$ is defined in the Appendix. The variance of the time domain signal, σ_{x}^2, can be calculated with the following formula for DCO-OFDM and U-OFDM:

$$\sigma_{\mathrm{x}}^2 = \frac{1}{N_{\mathrm{FFT}}} \sum_{j=0}^{N_{\mathrm{FFT}}-1} \log_2(M_j) E_{\mathrm{b}j}. \tag{29}$$

For ACO-OFDM and PAM-DMT, the time-domain variance can be calculated as:

$$\sigma_{\mathrm{x}}^2 = \frac{2}{N_{\mathrm{FFT}}} \sum_{j=0}^{N_{\mathrm{FFT}}-1} \log_2(M_j) E_{\mathrm{b}j} \tag{30}$$

where M_j is the size of the signal constellation and $E_{\mathrm{b}j}$ is the energy per bit at the jth subcarrier. The factor of two for ACO-OFDM and PAM-DMT results from the power rescaling after clipping of the negative samples. It should be noted that after pulse shaping, the variance of the oversampled signal is not constant over time. However, the authors of [12] have shown that for commonly used pulse shapes this does not influence the validity of the analysis. Results in this work confirm this finding. The calculations necessary to complete the statistical description of Y can be expressed as:

$$\begin{aligned}
\mathrm{E}[Y] = \mathrm{E}[\mathrm{z}(X)] &= \int_{-\infty}^{\infty} \mathrm{z}(x) \frac{1}{\sigma_{\mathrm{x}}} \phi\left(\frac{x}{\sigma_{\mathrm{x}}}\right) \mathrm{d}x \\
&= \int_{-\infty}^{\infty} \left\{ \sum_{l=1}^{|I|} \sum_{j=0}^{n_l} c_{l,j} x^j \left(\mathrm{U}(x - x_{\min,l}) \right.\right. \\
&\quad \left.\left. -\mathrm{U}(x - x_{\max,l})\right) \right\} \frac{1}{\sigma_{\mathrm{x}}} \phi\left(\frac{x}{\sigma_{\mathrm{x}}}\right) \mathrm{d}x \\
&= \sum_{l=1}^{|I|} \sum_{j=0}^{n_l} c_{l,j} \int_{x_{\min,l}}^{x_{\max,l}} x^j \frac{1}{\sigma_{\mathrm{x}}} \phi\left(\frac{x}{\sigma_{\mathrm{x}}}\right) \mathrm{d}x \\
&\overset{(46)}{=} \sum_{l=1}^{|I|} \sum_{j=0}^{n_l} c_{l,j} \left. \frac{\mathrm{d}^j \mathrm{D}(t, x_{\min,l}, x_{\max,l}, 0, \sigma_{\mathrm{x}})}{\mathrm{d}t^j} \right|_{t=0}
\end{aligned} \tag{31}$$

$$\begin{aligned}
\mathrm{E}[\mathrm{z}^2(X)] &= \int_{-\infty}^{\infty} \mathrm{z}^2(x) \frac{1}{\sigma_{\mathrm{x}}} \phi\left(\frac{x}{\sigma_{\mathrm{x}}}\right) \mathrm{d}x \\
&= \int_{-\infty}^{\infty} \left\{ \sum_{l=1}^{|I|} \sum_{j=0}^{n_l} c_{l,j} x^j \left(\mathrm{U}(x - x_{\min,l}) \right.\right. \\
&\quad \left.\left. -\mathrm{U}(x - x_{\max,l})\right) \right\}^2 \frac{1}{\sigma_{\mathrm{x}}} \phi\left(\frac{x}{\sigma_{\mathrm{x}}}\right) \mathrm{d}x \\
&= \sum_{l=1}^{|I|} \sum_{j=0}^{n_l} \sum_{k=0}^{n_l} c_{l,j} c_{l,k} \int_{x_{\min,l}}^{x_{\max,l}} x^{j+k} \frac{1}{\sigma_{\mathrm{x}}} \phi\left(\frac{x}{\sigma_{\mathrm{x}}}\right) \mathrm{d}x \\
&\overset{(46)}{=} \sum_{l=1}^{|I|} \sum_{j=0}^{n_l} \sum_{k=0}^{n_l} c_{l,j} c_{l,k} \left. \frac{\mathrm{d}^{j+k} \mathrm{D}(t, x_{\min,l}, x_{\max,l}, 0, \sigma_{\mathrm{x}})}{\mathrm{d}t^{j+k}} \right|_{t=0}
\end{aligned} \tag{32}$$

With the help of the Appendix and the standard differentiation rules, it is straightforward to obtain closed-form expressions for (28), (31) and (32). The procedure can easily be programmed on a computer. The resulting SNR at each frequency subcarrier can be calculated according to the following relationship:

$$\frac{E_{\mathrm{b}j}^{\mathrm{new}}}{\sigma_{\mathrm{NY}}^2} = \frac{\alpha^2 E_{\mathrm{b}j}}{\sigma_{\mathrm{N}}^2 + \sigma_{\mathrm{Y}}^2} \tag{33}$$

where $E_{\mathrm{b}j}^{\mathrm{new}}$ is the resulting energy per bit of the jth subcarrier, $E_{\mathrm{b}j}$ is the initial energy per bit of the jth subcarrier, σ_{N}^2 is the variance of the channel AWGN, and σ_{NY}^2 is the overall noise variance. Closed-form analytical expressions for the BER in M-PAM and M-QAM as a function of the SNR exist in the literature [20].

The Bussgang analysis presented so far is valid for zero-mean signals with Gaussian distribution. All four optical modulation schemes – DCO-OFDM, ACO-OFDM, PAM-DMT, U-OFDM – are modifications of the original zero-mean OFDM signal and need to be treated with care for a correct assessment of the nonlinearity effects. The analysis should take into account all effects on the signal up to the point where an FFT operation is performed by the OFDM demodulator at the receiver. Let's assume that $\mathrm{z}_1(x)$ is a memoryless distortion at one stage of the system, for example caused by clipping the signal within the allowed range; $\mathrm{z}_2(x)$ is a memoryless distortion at another stage, for example due to quantisation at the DAC; $\mathrm{z}_3(x)$ is a third memoryless distortion, for example the addition of a bias level. Then, the overall distortion after the three separate consecutive distortions is $\mathrm{z}(s'[t]) = \mathrm{z}_3(\mathrm{z}_2(\mathrm{z}_1(s'[t])))$. It does not matter whether a distortion is linear or nonlinear. It can always be incorporated in the analysis if it is memoryless. This work assumes that there is no distortion with memory or any such distortion can be completely equalised, for example ISI.

For comparison purposes, the average electrical energy per bit $E_{\mathrm{b,elec}}$ and the average optical energy per bit $E_{\mathrm{b,opt}}$ dissipated at the transmitter are defined as:

$$E_{\mathrm{b,elec}} = \frac{P_{\mathrm{elec}}^{\mathrm{avg}}}{B\eta} = \frac{\mathrm{E}[\mathrm{z}_{\mathrm{elec}}^2(s'[t])]}{B\eta} \tag{34}$$

$$E_{\mathrm{b,opt}} = \frac{P_{\mathrm{opt}}^{\mathrm{avg}}}{B\eta} = \frac{\mathrm{E}[\mathrm{z}_{\mathrm{opt}}(s'[t])]}{B\eta} \tag{35}$$

where $P_{\mathrm{elec}}^{\mathrm{avg}}$ is the average electrical power of the signal, proportional to the mean square of the electrical signal; $P_{\mathrm{opt}}^{\mathrm{avg}}$ is the average optical power of the signal, proportional to the average intensity of the optical signal; η is the respective spectral efficiency defined for the various schemes in (1), (7), (10) and (11); $\mathrm{z}_{\mathrm{elec}}(s'[t])$ is the current signal at the diode; $\mathrm{z}_{\mathrm{opt}}(s'[t])$ is the light intensity signal at the diode; B is the signal bandwidth in Hz. For the examples which are presented in this work, $\mathrm{z}_{\mathrm{elec}}(s'[t])$ includes clipping, quantisation effects at the DAC and biasing while $\mathrm{z}_{\mathrm{opt}}(s'[t])$ includes the current-to-light output characteristic of the diode in addition.

A. DCO-OFDM

The proposed analysis can be applied to DCO-OFDM in a straightforward manner. The biasing of the signal can be considered as part of the nonlinear transform. It does not need to be added separately like it has been done in other works [8], [10].

B. ACO-OFDM

The modulation process of ACO-OFDM includes clipping at zero. This operation is a nonlinear transform, but does not affect the odd carriers of the system. As a consequence, a slight modification needs to be made to the analysis in order to account for this effect. The modified approach is described in the rest of this section. In ACO-OFDM, the bipolar OFDM signal before clipping consists of a set of positive samples and a set of negative samples. The two sets have identical contribution to each modulated value in the frequency domain [3]. Therefore, setting one set to zero does not distort the useful signal except for a factor of 0.5. This means that the nonlinearity analysis can be conducted only on the positive samples. The result is the same as if the effect of a symmetrical distortion function on the bipolar OFDM signal is analysed. Hence, for the calculations, the intervals of the nonlinear transform can be specified from 0 to ∞. Then (28), (31) and (32) can be calculated in the interval $[0;\infty]$ and scaled by 2 to account for the negative half of the signal distribution. The equations become:

$$\alpha = \frac{2}{\sigma_{\mathrm{x}}^2}\sum_{l=1}^{|\mathrm{I}|}\sum_{j=0}^{n_l} c_{l,j}\left.\frac{\mathrm{d}^{j+1}\mathrm{D}(t,x_{\min,l},x_{\max,l},0,\sigma_{\mathrm{x}})}{\mathrm{d}t^{j+1}}\right|_{t=0} \tag{36}$$

$$\mathrm{E}[Y] = 2\sum_{l=1}^{|\mathrm{I}|}\sum_{j=0}^{n_l} c_{l,j}\left.\frac{\mathrm{d}^{j}\mathrm{D}(t,x_{\min,l},x_{\max,l},0,\sigma_{\mathrm{x}})}{\mathrm{d}t^{j}}\right|_{t=0} \tag{37}$$

$$\mathrm{E}[\mathrm{z}^2(X)] = \\ = 2\sum_{l=1}^{|\mathrm{I}|}\sum_{j=0}^{n_l}\sum_{k=0}^{n_l} c_{l,j}c_{l,k}\left.\frac{\mathrm{d}^{j+k}\mathrm{D}(t,x_{\min,l},x_{\max,l},0,\sigma_{\mathrm{x}})}{\mathrm{d}t^{j+k}}\right|_{t=0}. \tag{38}$$

The removal of the negative samples does not influence the odd subcarriers, as previously explained in Section III. The calculated noise variance, σ_{Y}^2, needs to be halved before addition to the AWGN variance because the noise is evenly distributed on both odd and even subcarriers. There is a 0.5 factor to the SNR, stemming from the removal of the negative samples. Then for ACO-OFDM, (33) becomes:

$$\frac{E_{\mathrm{b}j}^{\mathrm{new}}}{\sigma_{\mathrm{NY}}^2} = \frac{\alpha^2 E_{\mathrm{b}j}}{2(\sigma_{\mathrm{N}}^2 + \frac{\sigma_{\mathrm{Y}}^2}{2})}. \tag{39}$$

It should be noted that the zeroes from clipped negative samples need to preserve their value in order not to influence the modulated subcarriers. The overall distortion of the signal up to the demodulator is $\mathrm{z_d}(s'[t])$; this distortion does not include the addition of AWGN. If $\mathrm{z_d}(0) \neq 0$, then the zeros obtained from clipping the negative samples are distorted. The distortion on the clipped zero values in the time domain adds distortion on the odd subcarriers in the frequency domain. This effect is avoided when the clipped values are zero. If $\mathrm{z_d}(0)$ is interpreted as a DC shift and subtracted from $\mathrm{z_d}(s'[t])$, then the modified Bussgang analysis described in this section can be applied without having to additionally model the distortion resulting from the distorted clipped samples. Hence, the overall distortion, experienced by the nonzero ACO-OFDM samples is:

$$\mathrm{z}(s'[t])_{s'[t]\geq 0} = \mathrm{z_d}(s'[t])_{s'[t]\geq 0} - \mathrm{z_d}(0). \tag{40}$$

C. PAM-DMT

The time-domain signal of PAM-DMT has the same statistical properties as the ACO-OFDM signal. In addition, the power of the additive Gaussian noise from the nonlinearity is equally split between real and imaginary components in the frequency domain. Therefore, the nonlinearity analysis of PAM-DMT is exactly the same as for ACO-OFDM. It should be kept in mind that PAM-DMT employs M-PAM while ACO-OFDM employs M^2-QAM for the same spectral efficiency. In an additive Gaussian noise environment, M-PAM and M^2-QAM perform identically in terms of BER.

D. U-OFDM

In U-OFDM, the signs of negative samples are switched, they are transmitted as positive samples and switched back at the demodulator. As a result, the nonlinear distortion on the bipolar OFDM signal is symmetric around zero, *i.e.*, $\mathrm{z}(s'[t]) = -\mathrm{z}(-s'[t])$. Any two bipolar samples with the same absolute value experience exactly the same nonlinear distortion. Hence, $\mathrm{z}(s'[t])_{s'[t]\leq 0}$ is formed as a mirrored version of $\mathrm{z}(s'[t])_{s'[t]\geq 0}$ according to $\mathrm{z}(s'[t]) = -\mathrm{z}(-s'[t])$. Alternatively, it can be stated that due to the symmetry of the Gaussian probability density function (PDF), $\mathrm{z}(s'[t])$ can be specified only in the interval $[0;\infty]$ for the calculations of (28), (31) and (32). Each of the equations, however, needs to be doubled to account for the negative half of the distribution as is the case for ACO-OFDM and PAM-DMT. The subtraction of the negative block from the positive block effectively doubles the system AWGN. Hence (33) is modified as:

$$\frac{E_{\mathrm{b}j}^{\mathrm{new}}}{\sigma_{\mathrm{NY}}^2} = \frac{\alpha^2 E_{\mathrm{b}j}}{2\sigma_{\mathrm{N}}^2 + \sigma_{\mathrm{Y}}^2}. \tag{41}$$

It should be noted that in the demodulator the bipolar signal is obtained by subtracting the negative block from the positive one. If all zeroes corresponding to clipped negative samples from the original signal are transformed to $\mathrm{z_d}(0)\neq 0$, then the subtraction operation shifts all positive samples by $-\mathrm{z_d}(0)$ and all negative samples $\mathrm{z_d}(0)$. The function $\mathrm{z_d}(s'[t])$ is the overall nonlinearity distortion which the signal experiences on its path to the demodulator. The subtraction operation in the demodulation process effectively adds additional distortion, which needs to be accounted for by subtracting $\mathrm{z_d}(0)$ from $\mathrm{z_d}(s'[t])$, *i.e.*, the resulting overall nonlinearity becomes:

$$\mathrm{z}(s'[t])_{s'[t]\geq 0} = \mathrm{z_d}(s'[t])_{s'[t]\geq 0} - \mathrm{z_d}(0) \tag{42}$$

as in ACO-OFDM and PAM-DMT.

The analyses of ACO-OFDM, PAM-DMT, and U-OFDM show that all three schemes experience exactly the same SNR deterioration for the same nonlinearity effects. This occurs because the three schemes exhibit the same statistical properties in the time domain when their spectral efficiencies are equivalent. This finding is also supported by the results

in the next section. Therefore, in addition to the equivalent performance in a simple AWGN channel, the three schemes exhibit the same performance in a nonlinear AWGN channel.

VII. Numerical Results

In this section, the joint effect of three nonlinear distortions at the OWC transmitter is illustrated. These include clipping to account for the limited dynamic range of the electronic devices, quantisation from a low-resolution DAC, and the current-to-light output characteristic of the LED. Nonlinearities at the receiver are not examined since they are negligible in comparison to the ones present at the transmitter. They could be analysed in an analogous manner using the concepts presented in Section VI. In the following case study, the oversampled pulse-shaped signal $s'[t]$ has an oversampling ratio of 10.

The zero-order hold has a limited range of output amplitudes between ${s'}_{\min}$ and ${s'}_{\max}$, and a finite number of bits q. The different levels of the device are equally spaced in the interval $[{s'}_{\min}; {s'}_{\max}]$ at a distance of:

$$d_{\mathrm{q}} = \frac{{s'}_{\max} - {s'}_{\min}}{2^q - 1}. \tag{43}$$

Each quantisation threshold is set in the middle between two consecutive quantisation levels. For example, the threshold between ${s'}_{\min}$ and ${s'}_{\min} + d_{\mathrm{q}}$ is set at ${s'}_{\min} + d_{\mathrm{q}}/2$. The values of $s'_{\min}$ and $s'_{\max}$ are determined by the desired accuracy of the DAC and by the allowed operational range of the LED, $[i_{\min}; i_{\max}]$. Therefore, they account for the clipping effects introduced by the DAC and the LED. In the conducted simulations, the resolution of the DAC is set to q=8 bits.

After the signal values are quantised by the DAC output function, they are biased by a constant and are passed through the LED. The LED output function is a continuous function, specified in the interval $[i_{\min}; i_{\max}]$. According to the device datasheet [23], $i_{\min}$=0.1 A and $i_{\max}$=1 A. The LED output function corresponds to a transition from a current signal to an optical signal. The output characteristic of the LED has been obtained through interpolation of data from the device datasheet. A third degree polynomial has been used in the interpolation, and its coefficients are presented in Table I. The relationship between radiant flux (power) and luminous flux (power) is linear. Therefore, since only the relationship between current through the device and luminous flux is available in the datasheet, it has been adopted as an accurate representation of the relationship between the current and the radiation power.

It is assumed that the modulating signal is contained in the current signal through the LED. The initial average energy per bit of the original bipolar OFDM signal $s[n]$ is E_{b}. The actual dissipated electrical energy per bit at the LED assuming that the resistance is normalised to 1Ω and including the quantisation effects and biasing is $E_{\mathrm{b,elec}} = \mathrm{E}[i^2(t)]/(B\eta) = \mathrm{E}[(\mathrm{z}_3(\mathrm{z}_2(\mathrm{z}_1(s'[t]))) + i_{\mathrm{bias}})^2]/(B\eta)$. In this formula, $\mathrm{z}_1(s'[t])$ is the clipping effect in the preprocessing step applied on the oversampled pulse-shaped signal $s'[t]$; $\mathrm{z}_2(x)$ is the quantisation effect of the DAC; $\mathrm{z}_3(x)$ is the conversion from voltage to current, which is assumed to be linear with gain 1. In order to evaluate the optical efficiency of the system, a third quantity is defined as $E_{\mathrm{b,opt}} = \mathrm{E}[\mathrm{z}_4(\mathrm{z}_3(\mathrm{z}_2(\mathrm{z}_1(s'[t]))) + i_{\mathrm{bias}})]/(B\eta)$ where $\mathrm{z}_4(x)$ expresses the transition from current to optical signal in the LED, specified by the polynomial in Table I.

The modulation bandwidth of white-light LEDs is 2 MHz [19]. The coherence bandwidth of the optical channel is around 90 MHz [19], which is much higher than the modulation frequency of the LED. Hence, ISI does not need to be considered. In an alternative scenario, where ISI is an issue, the presented nonlinearity framework is still applicable as long as channel knowledge is available at the receiver, and the signal can be equalised. In the assumed system configuration, the received current signal can be expressed as:

$$\hat{i}(t) = \mathrm{z}_4(i(t)) h_{\mathrm{G}} \gamma \tag{44}$$

where h_{G} is the channel gain due to dispersion of light, and γ is the responsivity of the PD. Using the profile of the LED light spectrum and the PD responsivity to different optical wavelengths [24], the receiver responsivity to white light is calculated as $\gamma = 0.52$. The channel gain depends on a number of factors - distance, receiver area, angle with respect to the transmitter. In the current work, h_{G} is selected depending on the M-QAM modulation order that is used. The aim is to operate the LED in the full range of its active region because then the improvements of ACO-OFDM, PAM-DMT and U-OFDM over DCO-OFDM are demonstrated. In the cases when the optical signal varies only slightly around the biasing point, the energy consumption depends almost entirely on the biasing level, which makes the energy dissipation almost constant for the four schemes.

The main source of AWGN in an OWC system is shot noise at the photo detector caused by background light. The power spectral density of shot noise is N_{o}=10^{-21} W/Hz according to [19]. The variance of the AWGN is calculated as $\sigma^2_{\mathrm{N}} = BN_{\mathrm{o}}$.

Fig. 8 presents a working example which compares 4-QAM DCO-OFDM, 16-QAM ACO-OFDM, 4-PAM PAM-DMT, and 16-QAM U-OFDM – all with the same spectral efficiency of 1 bit/s/Hz. The simulated channel gain is h_{G}=4×10^{-6} since this value allows all the presented schemes to reach BER values in the order of 10^{-3} and 10^{-4} – required for successfull communication [10], [19]. At the same time, this value of the channel gain requires almost full utilisation of the LED active range. The bias levels for ACO-OFDM, PAM-DMT, and U-OFDM are set to i_{bias}=0.1 A since this is the minimum biasing requirement of the LED. The selected simulation parameters set the minimum bias level for DCO-OFDM at i_{bias}=0.19 A. The distribution region $[-3\sigma; 3\sigma]$ is quantised for DCO-OFDM, and the region $[0; 3\sigma]$ is quantised for the other three schemes. Anything outside those regions is clipped. These clipping levels are chosen to be the default clipping levels as they introduce negligible nonlinear distortion according to simulations. Since the AWGN power is constant, higher SNR values can be achieved by amplifying the information signal through the LED. However, if that signal falls outside the allowed operational range of the device when amplified, it is further clipped at the predistortion step in order to satisfy the electrical properties of the LED. Hence, the

TABLE I
POLYNOMIAL COEFFICIENTS $c_{l,k}$ IN INTERVAL l AND OF DEGREE k

Interval	$c_{l,3}$	$c_{l,2}$	$c_{l,1}$	$c_{l,0}$
$l = 1 \Leftrightarrow i(t) < i_{\min}$	0	0	0	0.1947
$l = 2 \Leftrightarrow i_{\min} < i(t) < i_{\max}$	0.2855	-1.0886	2.0565	-0.0003
$l = 3 \Leftrightarrow i_{\max} < i(t)$	0	0	0	1.2531

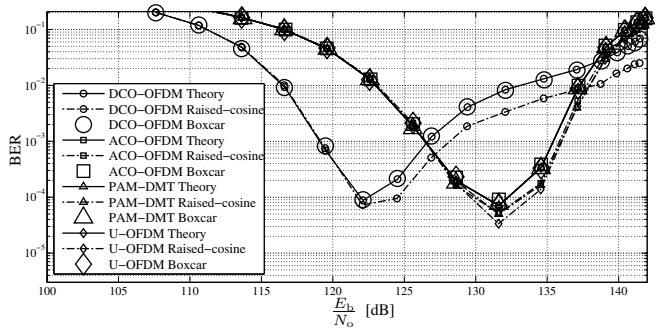

(a) Comparison of bipolar signals. Bias not taken into account.

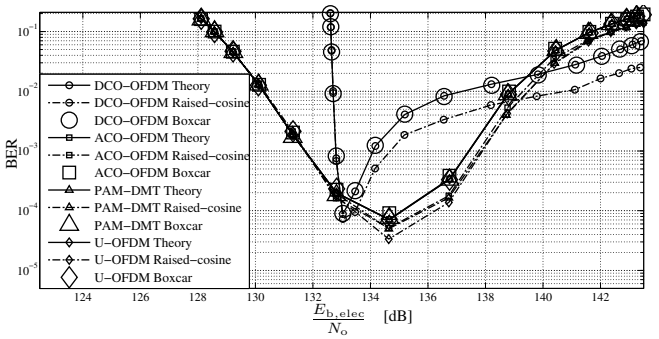

(b) Comparison of unipolar signals including contribution of bias to electrical power dissipation.

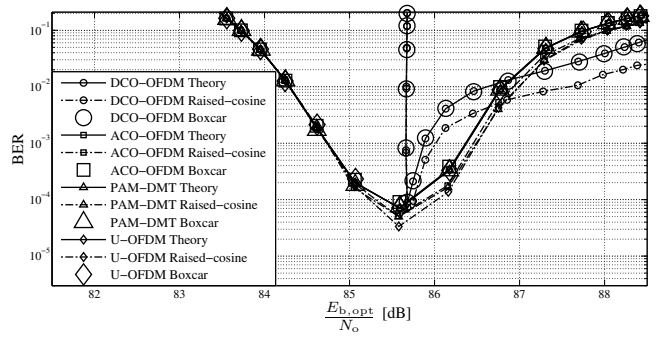

(c) Comparison of unipolar signals in terms of optical power requirements. Bias contribution to power dissipation included.

Fig. 8. Comparison between 4-QAM DCO-OFDM, 16-QAM ACO-OFDM, 4-PAM PAM-DMT, and 16-QAM U-OFDM in terms of electrical and optical SNR.

BER curves presented in this section are V-shaped. The dip in the plots emerges because after a certain point the distortion due to clipping outweighs the improvement due to the SNR increase. Fig. 8(a) shows the electrical energy efficiency of the four schemes when the energy dissipation due to biasing is neglected. As expected for bipolar signals, DCO-OFDM performs better than the other three schemes. The benefits of the latter, however, are due to the biasing requirement, and this can be observed in Fig. 8(b). In that figure, ACO-OFDM, PAM-DMT, and U-OFDM require about 1 dB less energy per bit than DCO-OFDM for $\mathrm{BER}{=}10^{-3}$ and about the same energy for $\mathrm{BER}{=}10^{-4}$. According to Fig. 8(c), DCO-OFDM is about 1 dB less optically efficient than the other three schemes for $\mathrm{BER}{=}10^{-3}$ and about 0.3 dB less efficient for $\mathrm{BER}{=}10^{-4}$. It is interesting to note that, as expected, the BER values decrease with the increase in SNR up to a certain point. Afterwards, the active region of the LED is exhausted, and the increase in power leads to increase in clipping and hence to more nonlinear distortion. It should also be noted that the theoretical analysis coincides well with the Monte Carlo simulation results for square pulse shapes (Boxcar filter). The Monte Carlo results for a root-raised-cosine filter are slightly better than the other results because the match filter at the receiver eliminates some of the distortion noise which falls outside the desired signal bandwidth. Nonetheless, the root-raised-cosine filter results follow closely the theoretical results and confirm validity of the new analytical framework. For practical purposes, the presented analysis can serve as a good lower bound approximation for the performance of systems which employ pulse shapes with limited bandwidth. To the best of the authors' knowledge, other available techniques for analysis of nonlinear distortion in OWC do not consider bandlimited pulse shapes. They assume simple square pulses (Boxcar filter) [6]–[10] for which an exact analysis is provided in this paper. The curves for ACO-OFDM, PAM-DMT and U-OFDM fall almost on top of each other as predicted by the theoretical analysis. This highlights the very similar performance of the three schemes.

ACO-OFDM, PAM-DMT, and U-OFDM exhibit better energy efficiency than DCO-OFDM. However, they require a bigger M-QAM constellation size for the same spectral efficiency. Larger constellations are more vulnerable to distortion. This vulnerability can put the three schemes at a disadvantage in certain scenarios. Such an example occurs if the channel gain is decreased to $h_{\mathrm{G}}{=}2{\times}10^{-6}$. In this case, the minimum biasing requirement of DCO-OFDM becomes $i_{\mathrm{bias}}{=}0.5$ A, and it is kept at $i_{\mathrm{bias}}{=}0.1$ A for the other three schemes. In spite of the worse performance in the previous simulation, in this scenario DCO-OFDM becomes the better choice. It is still able to achieve a BER of 10^{-4}, while all three other schemes cannot even reach a BER of 10^{-3}. This example shows that a minor change of the system parameters such as a factor of two in the channel gain can be decisive in the selection of a modulation scheme.

Fig. 9 presents a case for a significantly higher channel gain, $h_{\mathrm{G}}{=}4{\times}10^{-4}$. In this scenario, the information signal energy requirement is small. Hence, the main contributor to energy consumption is the biasing level. The bias of DCO-OFDM is

set to $i_{\mathrm{bias}} = 0.1018$ A, which is the minimum required bias that is able to accommodate the information signal without severe clipping distortion. The bias of the other three schemes is kept at the minimum, $i_{\mathrm{bias}} = 0.1$ A. The electrical energy advantage of ACO-OFDM, PAM-DMT, and U-OFDM over DCO-OFDM is in the order of 0.06 dB while the difference in the optical energy requirement is in the order of 0.04 dB. The four schemes are almost equivalent in performance because the main contributor to energy dissipation is the bias of the LED. It should be noted that the electrical energy efficiency of ACO-OFDM, PAM-DMT, and U-OFDM is lower than presented in the papers which originally introduced these concepts – [3], [4], [5]. The reason for this is that all clipped values which are set to zero at the modulator actually cannot be lower than the minimum required current at the LED and so also contribute to the power dissipation.

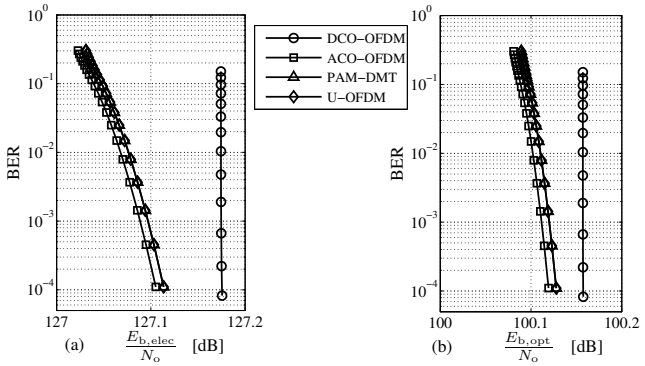

Fig. 9. Comparison of 4-QAM DCO-OFDM, 16-QAM ACO-OFDM, 4-QAM PAM-DMT, and 16-QAM U-OFDM for a high channel gain, $h_{\mathrm{G}}{=}4\times 10^{-4}$, scenario: (a) Electrical power efficiency including bias current; (b) Optical power efficiency including bias level.

The analysed schemes achieve higher spectral efficiency when the M-QAM/M-PAM modulation order is increased. This leads to more variance in the time-domain signal as described in (29) and (30), which for the same system parameters leads to more distortion. At the same time, bigger constellations are more sensitive to noise. Therefore, for higher spectral efficiencies and assuming the same OWC system parameters, the BER performance suffers from additional deterioration.

VIII. Conclusion

A complete analytical framework has been presented for the analysis of memoryless nonlinear distortion in an OWC system. It allows for the analysis of an arbitrary distortion function and guarantees closed-form solutions. The concept has been successfully applied to four separate OFDM-based modulation schemes proposed for IM/DD systems: DCO-OFDM, ACO-OFDM, PAM-DMT and U-OFDM. Examples have been given for the joint distortion effects from quantisation at a DAC element, as well as for distortion from the nonlinear relationship between electrical current and emitted light in an LED, which are the major sources of nonlinearity in an OWC system. Monte Carlo simulations show very good agreement with the proposed theory, thus confirming validity of the approach.

Analytical derivations as well as numerical results exhibit equivalent performance of ACO-OFDM, PAM-DMT, and U-OFDM in a nonlinear AWGN channel. The findings suggest that these schemes are three separate and equally valid approaches with respect to spectrum efficiency and energy efficiency. A brief analysis demonstrates that the optimal choice of a modulation scheme depends on the operating conditions and can change with variations in the system parameters. The presented framework provides a quick and accurate way to estimate system performance without computationally expensive Monte Carlo simulations and numerical integration. Thus, it enables system optimisation as the influence of a large range of system parameters can be evaluated exhaustively with reasonable computational complexity.

Appendix

This section presents the necessary formulas for derivation of a closed-form solution in the proposed novel analytical framework. The formulas are defined as follows:

$$\begin{aligned}
\mathrm{D}(t,a,b,\mu,\sigma_{\mathrm{x}}) &= \int_a^b e^{xt}\frac{1}{\sqrt{2\pi\sigma_{\mathrm{x}}^2}}e^{-\frac{(x-\mu)^2}{2\sigma_{\mathrm{x}}^2}}\,\mathrm{d}x\\
&= \int_a^b \frac{1}{\sqrt{2\pi\sigma_{\mathrm{x}}^2}}e^{-\frac{-2xt\sigma_{\mathrm{x}}^2+x^2-2\mu x+\mu^2}{2\sigma_{\mathrm{x}}^2}}\,\mathrm{d}x\\
&= \int_a^b \frac{1}{\sqrt{2\pi\sigma_{\mathrm{x}}^2}}e^{-\frac{x^2-2(t\sigma_{\mathrm{x}}^2+\mu)x+\mu^2}{2\sigma_{\mathrm{x}}^2}}\,\mathrm{d}x\\
&= \int_a^b \frac{1}{\sqrt{2\pi\sigma_{\mathrm{x}}^2}}e^{-\frac{x^2-2(t\sigma_{\mathrm{x}}^2+\mu)x+t^2\sigma_{\mathrm{x}}^4+2t\sigma_{\mathrm{x}}^2\mu+\mu^2-t^2\sigma_{\mathrm{x}}^4-2t\sigma_{\mathrm{x}}^2\mu}{2\sigma_{\mathrm{x}}^2}}\,\mathrm{d}x\\
&= e^{\frac{t^2\sigma_{\mathrm{x}}^2}{2}+t\mu}\int_a^b \frac{1}{\sqrt{2\pi\sigma_{\mathrm{x}}^2}}e^{-\frac{x^2-2(t\sigma_{\mathrm{x}}^2+\mu)x+(t\sigma_{\mathrm{x}}^2+\mu)^2}{2\sigma_{\mathrm{x}}^2}}\,\mathrm{d}x\\
&= e^{\frac{t^2\sigma_{\mathrm{x}}^2}{2}+t\mu}\int_a^b \frac{1}{\sqrt{2\pi\sigma_{\mathrm{x}}^2}}e^{-\frac{(x-\mu-t\sigma_{\mathrm{x}}^2)^2}{2\sigma_{\mathrm{x}}^2}}\,\mathrm{d}x\\
&= e^{\frac{t^2\sigma_{\mathrm{x}}^2}{2}+t\mu}\left(\mathrm{Q}\left(\frac{a-\mu-t\sigma_{\mathrm{x}}^2}{\sigma_{\mathrm{x}}}\right)-\mathrm{Q}\left(\frac{b-\mu-t\sigma_{\mathrm{x}}^2}{\sigma_{\mathrm{x}}}\right)\right)
\end{aligned} \tag{45}$$

where $\mathrm{Q}(x)$ is the tail probability of the standard normal distribution, and $\phi(x)$ is its PDF.

$$\begin{aligned}
\left.\frac{\mathrm{d}^n\mathrm{D}(t,a,b,\mu,\sigma_{\mathrm{x}})}{\mathrm{d}t^n}\right|_{t=0} &\overset{(45)}{=}\\
&= \left.\frac{\mathrm{d}^n}{\mathrm{d}t^n}\int_a^b e^{xt}\frac{1}{\sqrt{2\pi\sigma_{\mathrm{x}}^2}}e^{-\frac{(x-\mu)^2}{2\sigma_{\mathrm{x}}^2}}\,\mathrm{d}x\right|_{t=0}\\
&= \left.\int_a^b \frac{\mathrm{d}^n}{\mathrm{d}t^n}e^{xt}\frac{1}{\sqrt{2\pi\sigma_{\mathrm{x}}^2}}e^{-\frac{(x-\mu)^2}{2\sigma_{\mathrm{x}}^2}}\,\mathrm{d}x\right|_{t=0}\\
&= \left.\int_a^b x^n e^{xt}\frac{1}{\sqrt{2\pi\sigma_{\mathrm{x}}^2}}e^{-\frac{(x-\mu)^2}{2\sigma_{\mathrm{x}}^2}}\,\mathrm{d}x\right|_{t=0}\\
&= \int_a^b x^n\frac{1}{\sqrt{2\pi\sigma_{\mathrm{x}}^2}}e^{-\frac{(x-\mu)^2}{2\sigma_{\mathrm{x}}^2}}\,\mathrm{d}x
\end{aligned} \tag{46}$$

$$\frac{\mathrm{dQ}\left(\frac{x-\mu-t\sigma_{\mathrm{x}}^2}{\sigma_{\mathrm{x}}}\right)}{\mathrm{d}t} = \phi\left(\frac{x-\mu-t\sigma_{\mathrm{x}}^2}{\sigma_{\mathrm{x}}}\right)\sigma_{\mathrm{x}} \tag{47}$$

$$\frac{\mathrm{d}\phi\left(\frac{x-\mu-t\sigma_{\mathrm{x}}^2}{\sigma_{\mathrm{x}}}\right)}{\mathrm{d}t} = \phi\left(\frac{x-\mu-t\sigma_{\mathrm{x}}^2}{\sigma_{\mathrm{x}}}\right)\left(\frac{x-\mu-t\sigma_{\mathrm{x}}^2}{\sigma_{\mathrm{x}}}\right)\sigma_{\mathrm{x}} \tag{48}$$

REFERENCES

[1] "Visible Light Communication (VLC) - A Potential Solution to the Global Wireless Spectrum Shortage," GBI Research, Tech. Rep., 2011. [Online]. Available: http://www.gbiresearch.com/

[2] J. A. C. Bingham, "Multicarrier Modulation for Data Transmission: an idea whose time has come," *IEEE Communications Magazine*, vol. 28, no. 5, pp. 5–14, May 1990.

[3] J. Armstrong and A. Lowery, "Power Efficient Optical OFDM," *Electronics Letters*, vol. 42, no. 6, pp. 370–372, Mar. 16, 2006.

[4] S. C. J. Lee, S. Randel, F. Breyer, and A. M. J. Koonen, "PAM-DMT for Intensity-Modulated and Direct-Detection Optical Communication Systems," *IEEE Photonics Technology Letters*, vol. 21, no. 23, pp. 1749–1751, Dec. 2009.

[5] D. Tsonev, S. Sinanović, and H. Haas, "Novel Unipolar Orthogonal Frequency Division Multiplexing (U-OFDM) for Optical Wireless," in *Proc. of the Vehicular Technology Conference (VTC Spring)*, IEEE. Yokohama, Japan: IEEE, May 6–9 2012.

[6] I. Neokosmidis, T. Kamalakis, J. W. Walewski, B. Inan, and T. Sphicopoulos, "Impact of Nonlinear LED Transfer Function on Discrete Multitone Modulation: Analytical Approach," *Lightwave Technology*, vol. 27, no. 22, pp. 4970–4978, 2009.

[7] H. Elgala, R. Mesleh, and H. Haas, "A Study of LED Nonlinearity Effects on Optical Wireless Transmission using OFDM," in *Proceedings of the* 6^{th} *IEEE International Conference on wireless and Optical communications Networks (WOCN)*, Cairo, Egypt, Apr. 28–30, 2009.

[8] S. Dimitrov, S. Sinanovic, and H. Haas, "Clipping Noise in OFDM-based Optical Wireless Communication Systems," *IEEE Transactions on Communications (IEEE TCOM)*, vol. 60, no. 4, pp. 1072–1081, Apr. 2012.

[9] H. Elgala, R. Mesleh, and H. Haas, "Impact of LED nonlinearities on optical wireless OFDM systems," in *2010 IEEE 21st International Symposium on Personal Indoor and Mobile Radio Communications (PIMRC)*, sept 2010, pp. 634 – 638.

[10] S. Dimitrov, S. Sinanovic, and H. Haas, "Signal Shaping and Modulation for Optical Wireless Communication," *IEEE/OSA Journal on Lightwave Technology (IEEE/OSA JLT)*, vol. 30, no. 9, pp. 1319–1328, May 2012.

[11] N. Fernando, Y. Hong, and E. Viterbo, "Flip-OFDM for Optical Wireless Communications," in *Information Theory Workshop (ITW)*, IEEE. Paraty, Brazil: IEEE, Oct., 16–20 2011, pp. 5–9.

[12] D. Dardari, V. Tralli, and A. Vaccari, "A Theoretical Characterization of Nonlinear Distortion Effects in OFDM Systems," *IEEE Transactions on Communications*, vol. 48, no. 10, pp. 1755–1764, Oct. 2000.

[13] A. Bahai, M. Singh, A. Goldsmith, and B. Saltzberg, "A New Approach for Evaluating Clipping Distortion in Multicarrier Systems," *IEEE Journal on Selected Areas in Communications*, vol. 20, no. 5, pp. 1037–1046, Jun. 2002.

[14] X. Li and J. Cimini, L.J., "Effects of Clipping and Filtering on the Performance of OFDM," *IEEE Communications Letters*, vol. 2, no. 5, pp. 131–133, May 1998.

[15] D. J. G. Mestdagh, P. Spruyt, and B. Biran, "Analysis of Clipping Effect in DMT-based ADSL Systems," in *Proc. IEEE International Conference on Communications ICC 1994*, vol. 1, New Orleans, LA, USA, 1–5 May 1994, pp. 293–300.

[16] B. Inan, S.C.J. Lee, S. Randel, I. Neokosmidis, A.M.J. Koonen and J.W. Walewski, "Impact of LED Nonlinearity on Discrete Multitone Modulation," *IEEE/OSA Journal of Optical Communications and Networking*, vol. 1, no. 5, pp. 439 –451, oct 2009.

[17] H. Elgala, R. Mesleh, and H. Haas, "Indoor Optical Wireless Communication: Potential and State-of-the-Art," *IEEE Commun. Mag.*, vol. 49, no. 9, pp. 56–62, Sep. 2011, ISSN: 0163-6804.

[18] D. Tsonev, S. Sinanović, and H. Haas, "Enhanced Subcarrier Index Modulation (SIM) OFDM," in *Proc. of the MMCOM'11 Workshop in conjuction with the Global Communications Conference (GLOBECOM)*, IEEE. Houston, Texas, USA: IEEE, Dec. 5–9, 2011.

[19] J. Grubor, S. Randel, K. Langer, and J. Walewski, "Bandwidth Efficient Indoor Optical Wireless Communications with White Light Emitting Diodes," in *In the Proceeding of the* 6^{th} *International Symposium on Communication Systems, Networks and Digital Signal Processing*, vol. 1, Graz, Austria, Jun. 23–25, 2008, pp. 165–169.

[20] J. G. Proakis and D. K. Manolakis, *Digital Signal Processing: Principles, Algorithms and Application*, 4th ed., T. Robbins, Ed. Prentice Hall, Apr. 2006.

[21] J. Bussgang, "Cross Correlation Function of Amplitude-Distorted Gaussian Signals," Research Laboratory for Electronics, Massachusetts Institute of Technology, Cambridge, MA, Technical Report 216, Mar. 1952.

[22] H. E. Rowe, "Memoryless Nonlinearities With Gaussian Inputs: Elementary Results," *The Bell System Technical Journal*, vol. 61, no. 7, pp. 1519 – 1525, Sep. 1982.

[23] OSRAM GmbH, "Datasheet: OS-PCN-2008-002-A OSTAR LED," Retrieved from http://www.osram.de, Feb. 2008.

[24] Vishay Semiconductors, "Datasheet: BPV10 Silicon PIN Photodiode, RoHS Compliant," Retrieved Aug 01, 2012 from www.vishay.com/docs/81502/bpv10.pdf, Aug. 2012.

Dobroslav Tsonev (S'11) received the BSc degree in electrical engineering and computer science in 2008 from Jacobs University Bremen, Bremen, Germany and the MSc degree in communication engineering with a specialisation in electronics in 2010 from the Munich Institute of Technology, Munich, Germany. Currently, he is pursuing a PhD degree in electrical engineering at the University of Edinburgh. His main research interests lie in the area of optical wireless communication with an emphasis on visible light communication.

Sinan Sinanovic (S'98-M'07) is a lecturer at Glasgow Caledonian University. He has obtained his Ph.D. in electrical and computer engineering from Rice University, Houston, Texas, in 2006. In the same year, he joined Jacobs University Bremen in Germany as a post doctoral fellow. In 2007, he joined the University of Edinburgh in the UK where he has worked as a research fellow in the Institute for Digital Communications. While working with Halliburton Energy Services, he has developed acoustic telemetry receiver which was patented. He has also worked for Texas Instruments on development of ASIC testing. He is a member of the Tau Beta Pi engineering honor society and a member of Eta Kappa Nu electrical engineering honor society. He won an honourable mention at the International Math Olympiad in 1994.

Prof. Harald Haas (S'98-A'00-M'03) holds the Chair of Mobile Communications in the Institute for Digital Communications (IDCOM) at the University of Edinburgh, Edinburgh, U.K., and he currently is the CSO of a university spin-out company pureVLC Ltd. His main research interests are in interference coordination in wireless networks, spatial modulation, and optical wireless communication. He holds more than 23 patents. He has published more than 50 journal papers including a Science article and more than 170 peer-reviewed conference papers. Nine of his papers are invited papers. He has co-authored a book entitled Next Generation Mobile Access Technologies: Implementing TDD (Cambridge, U.K.: Cambridge Univ. Press, 2008). Since 2007, he has been a Regular High Level Visiting Scientist supported by the Chinese 111 program at Beijing University of Posts and Telecommunications (BUPT). Prof. Haas was an invited speaker at the TED Global conference 2011, and his work on optical wireless communication was listed among the 50 best inventions in 2011 in Time Magazine. In 2011 he has received a prestigious Fellowship of the Engineering and Physical Sciences Research Council (EPSRC) in the UK.